

A model of anthrax toxin lethal factor bound to protective antigen

D. Borden Lacy*, Henry C. Lin*, Roman A. Melnyk*, Ora Schueler-Furman[†], Laura Reither[‡], Kristina Cunningham*[§], David Baker^{†¶}, and R. John Collier*^{||}

*Department of Microbiology and Molecular Genetics and [‡]Graduate Group of Biological Chemistry and Molecular Pharmacology, Harvard Medical School, 200 Longwood Avenue, Boston, MA 02115; and [†]Department of Biochemistry and [¶]Howard Hughes Medical Institute, University of Washington, Seattle, WA 98195

Contributed by R. John Collier, September 21, 2005

Anthrax toxin is made up of three proteins: the edema factor (EF), lethal factor (LF) enzymes, and the multifunctional protective antigen (PA). Proteolytically activated PA heptamerizes, binds the EF/LF enzymes, and forms a pore that allows for EF/LF passage into host cells. Using directed mutagenesis, we identified three LF-PA contact points defined by a specific disulfide crosslink and two pairs of complementary charge-reversal mutations. These contact points were consistent with the lowest energy LF-PA complex found by using Rosetta protein-protein docking. These results illustrate how biochemical and computational methods can be combined to produce reliable models of large complexes. The model shows that EF and LF bind through a highly electrostatic interface, with their flexible N-terminal region positioned at the entrance of the heptameric PA pore and thus poised to initiate translocation in an N- to C-terminal direction.

computation | docking | electrostatic

B*acillus anthracis*, the causative agent of anthrax, secretes three monomeric proteins, protective antigen (PA), edema factor (EF), and lethal factor (LF), that are collectively referred to as anthrax toxin (1). After its proteolytic activation and assembly into oligomeric complexes, PA can mediate the delivery of the two catalytic factors, EF and LF, into the host cell cytosol, where they can access their substrates. EF, an 89-kDa calmodulin-dependent adenylate cyclase, elevates levels of cAMP (2). LF, named for its lethal effect in animals, is a 90-kDa zinc protease that has been shown to cleave and inactivate mitogen-activated protein kinase-kinases (3, 4).

The current model for intoxication involves a multistep mechanism, the first step being binding of the 83-kDa PA monomer (PA₈₃) to a host-cell surface receptor (1). Binding is followed by proteolytic cleavage of PA₈₃, resulting in the removal of a 20-kDa fragment (PA₂₀) from the N terminus (5). The remaining 63-kDa PA (PA₆₃) is then able to oligomerize, forming a heptameric, soluble prepore (6), which, in turn, binds a maximum of three molecules of EF and/or LF (7). The limit of three has been proposed to derive from EF and LF having a footprint of binding that encompasses two PA₆₃ subunits (8). The entire complex of the (PA₆₃)₇ prepore and bound catalytic factor(s) is internalized into an endosome by receptor-mediated endocytosis (9). The increasing acidity of the endosome causes a conformational change in the prepore assembly, allowing it to penetrate the endosomal membrane and form a pore (1). This pore is thought to allow for the translocation of fully or partially unfolded EF or LF through the endosomal membrane into the cytosol, where catalysis can occur (10, 11).

EF and LF have entirely different catalytic activities but share at their N termini a common domain with significant sequence and structural homology (12, 13). This domain, referred to as EF_N or LF_N, contains the site that allows EF and LF to bind PA competitively and with high affinity ($K_d \approx 1$ nM) (14). EF_N and LF_N share a cluster of seven conserved amino acids that were shown by site-directed mutagenesis and a cell-surface binding

assay to be important for binding PA (15). These residues form a relatively flat surface with dimensions of ≈ 10 – 15 Å (Fig. 1*a*). Two of the seven amino acids are Asp residues and are likely to give the binding site a net negative charge.

Binding of EF/LF depends on and potentially drives the oligomerization of PA₆₃ (16). This interaction was discovered through the use of two oligomerization-deficient forms of PA, each mutated on a different PA₆₃–PA₆₃ contact face. Neither form of PA alone is able to oligomerize or bind ligand, either in solution or on cells. However, when the two mutant forms of PA are combined, there is one wild-type interface that allows for dimer formation in the presence of ligand. The discovery that stable PA₆₃–PA₆₃ dimers formed only in the presence of ligand led to the hypothesis that the EF/LF-binding site spanned two PA₆₃ subunits. Mutations were introduced into each of the two oligomerization-deficient forms of PA to map the single ligand-binding site within dimeric PA (8). The results suggested that the EF/LF-binding site was formed by two clusters of residues separated by ≈ 30 Å in the PA dimer (Fig. 1*b*). The two clusters are located on a relatively flat surface and are positively charged, because combined they contain three Arg and three Lys residues.

In this study, we docked LF_N across a PA-dimer interface in two distinct orientations and evaluated these models computationally by using only their computed energies. Independently, we explored the binding by directed mutagenesis. Cys-scanning mutagenesis revealed a site where a specific disulfide crosslink can form between bound LF_N and PA, and we also found two pairs of electrostatic interactions by charge-reversal mutagenesis. The three contact points identified by the mutational analysis define a single orientation of LF_N, and this orientation coincides with the lowest energy model that emerged from the computational analysis. The binding orientation yields insights into the subsequent steps of the entry process of LF and EF, including their unfolding and translocation through the PA pore.

Materials and Methods

Modeling the Structure of the LF_N–PA Dimer Complex. To reduce computational time, the PA₆₃–PA₆₃ dimer was truncated to include residues 177–260 (the subdomain that contains the EF/LF-binding site) and 458–595 (a subdomain that mediates oligomerization). The manually docked models were used as a starting point for sampling the surrounding free energy landscape by using many independent Monte Carlo minimization trajectories according to a Rosetta-Dock protocol described in refs. 17 and 18. Briefly, the rigid degrees of freedom of the starting model are randomly perturbed, and the perturbed model

Conflict of interest statement: R.J.C. holds equity in PharmAthene, Inc., a company engaged in developing countermeasures to biothreat agents, including *Bacillus anthracis*.

Abbreviations: EF, edema factor; LF, lethal factor; PA, protective antigen; rmsd, rms deviation.

[§]Present address: Wyeth Research, Cambridge, MA 02140.

^{||}To whom correspondence should be addressed. E-mail: john.collier@hms.harvard.edu.

© 2005 by The National Academy of Sciences of the USA

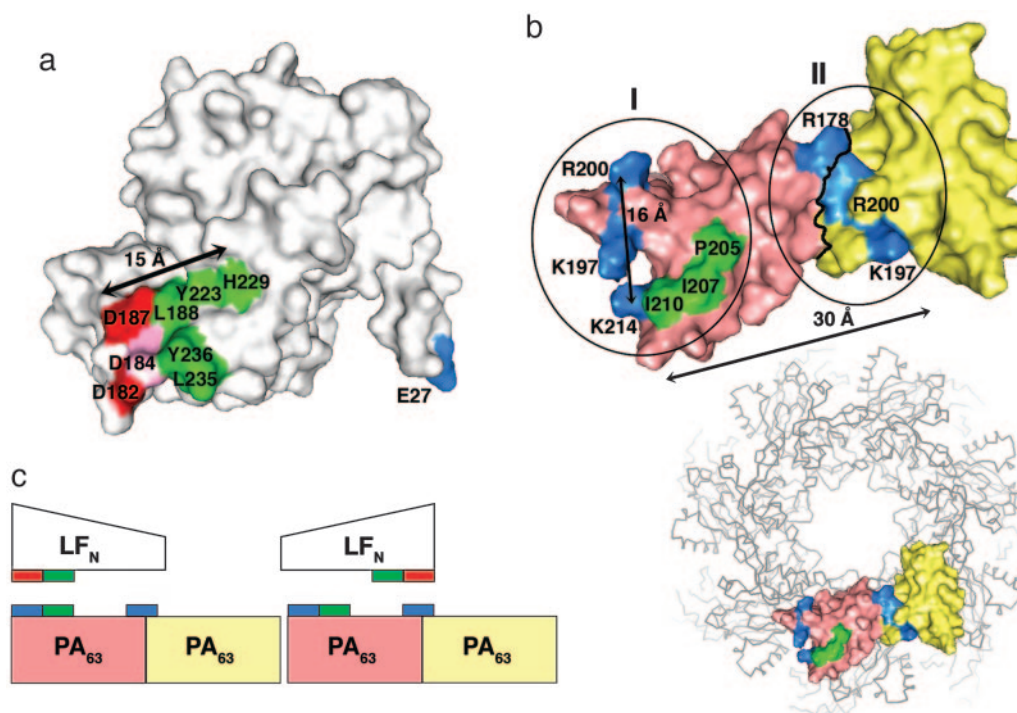


Fig. 1. Mapping the PA- and LF-binding sites by site-directed mutagenesis. (a) The seven residues important for binding PA (D182, D187, L188, Y223, H229, L235, and Y236) cluster on the surface of LF_N and are shown in green and red (15). (The D184A mutant did not show a binding defect but is depicted in pink, because it is likely to contribute to a net negative charge in this region.) Approximate dimensions of the site are indicated by the D187 C α –H229 C α distance (15 Å). The N terminus of the domain (E27) is shown in blue. (b) A surface rendering of the N-terminal domain 1' (residues 175–258) from two PA₆₃ subunits (yellow and pink) as viewed from the top of the heptameric ring. LF_N binding studies to dimeric PA₆₃ suggested two clusters of important residues shown in green and blue (8). One cluster contains residues P205, I207, I210, K214, K197, and R200 (subsite I). The second cluster contains R178 and the K197 and R200 residues from the neighboring PA₆₃ subunit (subsite II). (Note: The P205A mutant was not tested in the dimeric background but is likely part of the first subsite because of its proximity to I207. K197 and R200, which were originally tested only in the context of subsite II, have recently been shown to participate in subsite I as well; H.C.L., unpublished work.) Approximate dimensions of the site are indicated by distances of the K214 C α to the R200 C α of the same subunit (16 Å) and the neighboring subunit (30 Å). Coordinates for LF_N and the PA₆₃–PA₆₃ dimer were obtained from the 1J7N (12) and 1TZO (25) crystal structures, respectively. (c) LF_N was manually docked on the PA dimer in two orientations that differed by $\approx 180^\circ$.

is subjected first to low-resolution refinement and then to high-resolution refinement. In the high-resolution refinement step, the side-chain and backbone degrees of freedom are optimized simultaneously in the context of a detailed all-atom energy function dominated by short-range hydrogen bonding, van der Waals interactions, and desolvation. The rms deviation (rmsd) values were calculated over the LF_N molecule after superposition of the PA dimer with the starting model.

Preparation of PA, LF_N, and Mutants. Oligonucleotides were synthesized by Integrated DNA Technologies (Coralville, IA). Mutations in PA and LF_N were made in the pET22b-PA (1–735) (19) and pET15b-LF_N (1–263) (15) constructs, respectively, by using the QuikChange method (Stratagene) of site-directed mutagenesis. ³⁵S-labeled LF_N proteins were produced by *in vitro* transcription/translation by using a TNT coupled reticulocyte lysate system (Promega). Otherwise, PA and LF_N were expressed and purified from *Escherichia coli* as described in refs. 20 and 21. PA was activated by using a trypsin-to-PA ratio of 1:1,000 (wt/wt). The mixture was incubated at room temperature for 30 min and quenched with a 10 M excess of soybean trypsin inhibitor.

Disulfide Crosslinking. Activated PA was incubated with an equimolar amount of LF_N in the presence of excess DTT for 1 h on ice to allow for binding. The PA–LF_N mixture was applied to a Sephadex G-25 column (Amersham Pharmacia) to remove DTT and exchange the complex into a buffer containing 50 mM

NaCl and 20 mM Tris-Cl (pH 8.0). Samples were allowed to oxidize for 10 min before adding *N*-ethylmaleimide to quench any remaining free cysteines. The proteins were precipitated with trichloroacetic acid, resuspended in SDS buffer, and then analyzed by SDS/PAGE using a 7.5% acrylamide/SDS gel. Gels were stained with Coomassie blue.

Binding Assay for Charge-Reversal Mutants. PA-mediated binding of ³⁵S-labeled LF_N was performed on CHO-K1 cells (CCL-61, American Type Culture Collection) as described in ref. 22. Supplies for cell culture media were from Invitrogen. Cells were grown in Ham's F-12 medium supplemented with 10% calf serum, 500 units/ml penicillin G, and 500 units/ml streptomycin sulfate and were maintained as monolayers in a humidified atmosphere of 5% CO₂. The cells (2×10^5 cells per well) were incubated on ice with 2.4×10^{-8} M trypsin-nicked PA for 1 h. The cells were washed with PBS and incubated on ice with ³⁵S-labeled LF_N for 1 h. Cells were washed three times with PBS and treated with lysis buffer, and the radioactive content was determined by scintillation counting.

Results

Creating a Model of LF_N Bound to a PA Dimer. LF_N was manually docked on a truncated PA dimer in two orientations that differed by $\approx 180^\circ$ (Fig. 1c). In the first orientation (Fig. 1c *Left*), the PA-binding site on LF_N was aligned to subsite I of PA to maximize both the charge complementarity between the negatively and positively charged amino acids and the overlap of

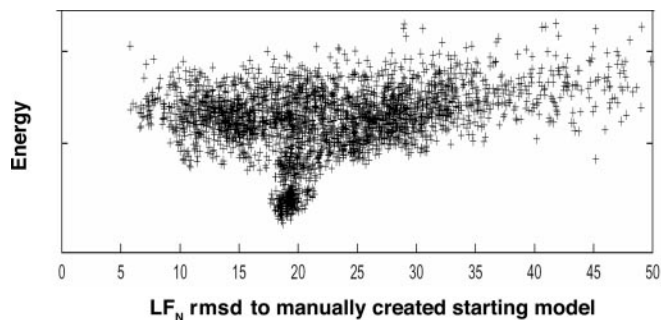


Fig. 2. The Rosetta-Dock model of the LF_N-PA dimer complex lies in a deep energy funnel. Three thousand independent trajectories were carried out, starting from the manually docked model. The energy for each structure (arbitrary units) is plotted against the rmsd between LF_N molecules when the PA subunits from the manually docked and final models are aligned. There is a dramatic energy funnel around 20 Å from the starting model. The lowest energy structure also is the center of the largest cluster of low-energy models, and it is our most reliable model for this complex.

hydrophobic residues. In the second orientation (Fig. 1c Right), the negatively charged residues of the LF_N PA-binding site were aligned to PA subsite II. Both models were then subjected to refinement by using the Rosetta-Dock protocol. To sample the free-energy landscape in the vicinity of the manually docked models, we carried out 3,000 independent refinement trajectories starting from random perturbations of the starting models (see *Materials and Methods*). Whereas the refinement of models from the second orientation did not result in an energetic minimum (data not shown), the energy landscape produced by the refinement from the first orientation (Fig. 2) contained a pronounced energy minimum. Alignment of the PA dimers indicates that, in these low-energy models, LF_N differs from the starting model by ≈20 Å rmsd. Dramatic energy funnels, such as this one, were found post facto to be strong indicators of the correctness of a prediction in the double-blind Critical Assessment of Predicted Interactions (CAPRI) protein-protein docking experiment in which a number of the predictions made by using the Rosetta-Dock protocol turned out to have close to atomic-level accuracy (18, 23). We chose the lowest energy model generated, the lowest energy point in Fig. 2, as our prediction. It should be emphasized that the model was selected based on energy criteria alone, and that no experimental information was used other than that implicit in the manually docked starting structures.

Identification of a Disulfide Crosslink Between LF_N Y108C and PA N209C. Because neither LF nor PA contains cysteine, introducing cysteines by site-directed mutagenesis represents a straightforward method to test for formation of disulfide crosslinks with binding. First, heptameric, wild-type PA₆₃ or PA₆₃ N209C was incubated with wild-type LF_N or one of seven LF_N mutants: Y108C, K110C, Y118C, Q132C, S134C, D136C, and Q228C. Binding was allowed to occur in the presence of excess DTT to prevent the formation of nonspecific disulfides. The DTT was then removed, and the samples were allowed to oxidize briefly before being treated with *N*-ethylmaleimide. The formation of a disulfide crosslink between LF_N Y108C and PA₆₃ N209C was visible as a slow-mobility band on an SDS gel that could be disrupted in the presence of DTT (Fig. 3). This band was shown by Western blotting with anti-PA and anti-LF_N antibodies to contain both PA and LF_N (data not shown). The crosslink formed selectively, because LF_N K110C, Y118C, Q132C, S134C, D136C, and Q228C did not form crosslinks when incubated with PA₆₃ N209C (data not shown). Likewise, LF_N Y108C did not crosslink with PA₆₃ S186C (data not shown).

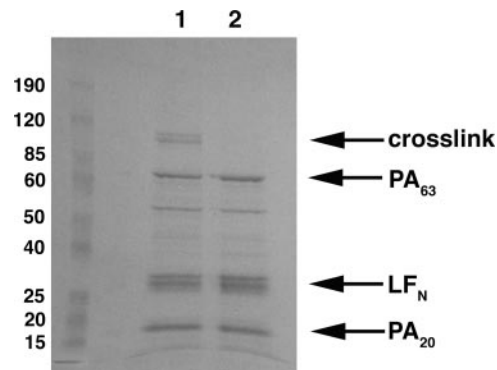


Fig. 3. Identification of a disulfide crosslink between LF_N Y108C and PA N209C. LF_N Y108C and PA₆₃ N209C form a disulfide-linked complex under oxidizing conditions (lane 1), which is disrupted in the presence of 10 mM DTT (lane 2).

Identification of Complementary Charge-Reversal Mutations That Can Rescue Binding. The LF_N- and PA-binding surfaces are notable in that they contain a large number of negatively and positively charged residues, respectively. The idea that electrostatics might play an important role in the binding interaction suggested that it might be possible to exchange a specific negative residue in LF_N and a positive residue in PA in a way that would not compromise the binding interaction.

Reversing the charge in six of the positively charged residues of PA (R178D, K197D, R200E, K213E, K214E, and K218E) inhibited binding of wild-type LF_N, (binding was observed at 0–63% of wild-type levels, Fig. 4). Similarly, substituting a lysine for LF_N D187 reduced PA-binding to 3% of wild-type levels. Pairing the LF_N D187K mutant with each of the six PA charge-reversal mutants restored binding to 120% of wild-type levels in the case of the LF_N D187K-PA K213E pair but had no significant effect on the other five PA mutants (Fig. 4). After identifying the LF_N D187K-PA K213E pair, LF_N D187K also

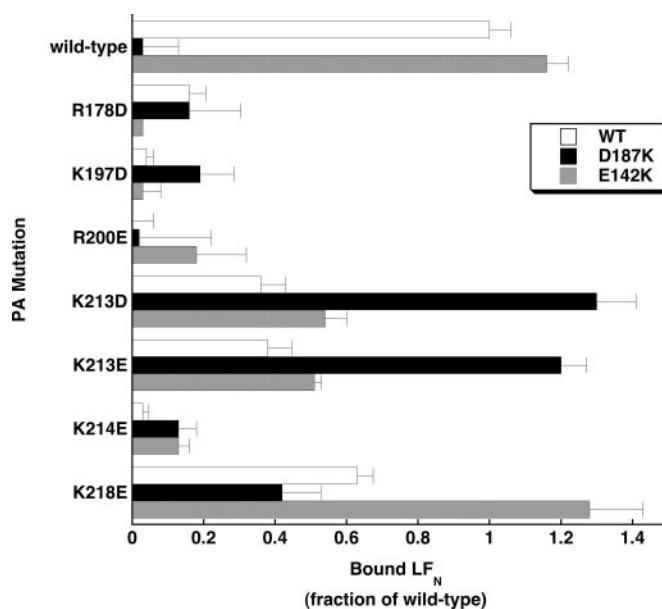


Fig. 4. A cell-surface binding assay shows that the LF_N D187K-PA K213D/K213E and LF_N E142K-PA K218E pairs can rescue binding defects. Data represent the fraction of mutant ³⁵S-labeled LF_N bound specifically to PA on cells relative to that of wild-type LF_N. Error bars represent SEM.

partner protein and reasoned that pairing these charge-reversal mutants so that they could maintain an electrostatic interaction might rescue binding for these otherwise defective mutants. We identified two such pairs of charge-reversal mutants: LF_N D187K–PA K213D/K213E and LF_N E142K–PA K218E, suggesting that the LF_N D187–PA K213 and LF_N E142–PA K218 residues are close in the LF_N–PA complex (Fig. 4). In the low-energy model, the charge pairs are located on either side of the disulfide crosslink (Fig. 5a). Although the Rosetta-Dock protocol does not emphasize electrostatics, the model suggests that, with modest rearrangement of side chain rotamers, these pairs of residues should be close enough to form favorable electrostatic interactions.

Alignment of the PA molecules from the energetically favorable model and its starting model reveals that LF_N has shifted by a rmsd of 20 Å. This large departure from the starting model is because of a twist in LF_N that unexpectedly minimizes the interaction of LF_N with PA subsite II. As modeled, LF_N contacts the K197 residue of the PA₆₃–PA₆₃ interface but does not make any direct contacts with R178 and R200 (the two other residues of the second subsite suggested by the mutagenesis work done in the PA dimer; ref. 8) (Figs. 1b and 5c). We found that it was not possible to identify an alternate low-energy model in which LF_N could interact with these residues. One possibility is that there is a conformational change in LF_N and/or PA that could not be modeled by using rigid backbone structures. We now question, however, whether LF_N-dependent dimerization of the oligomerization-deficient PA mutants yielded an unambiguous map of binding defects. Because R178, K197, and R200 are located at the dimer interface, it is possible that mutation of these residues causes oligomerization defects and does not directly affect ligand binding. Because PA dimers are formed only in the presence of ligand, it is difficult to distinguish these two possibilities. Given that the subsite II data may not reflect LF_N binding and that the model recapitulates the independently identified disulfide and electrostatic pairs, we propose the low-energy model as a reliable prediction of the LF_N–PA dimer complex structure. The fact that a purely energy-based prediction can reproduce the experimental results quite well and even point at possible incorrect information is encouraging and demonstrates that high-resolution structure prediction can make useful contributions to the structural characterization of a protein–protein interface, particularly in conjunction with experimental data. The combination of experimental and computational methods in this study may represent the beginning of a new paradigm for structure determination as computational methods become more accurate and structural biologists seek to understand larger and more complex systems that are less amenable to traditional high-resolution structure-determination methods.

The energetically favorable model has LF_N spanning two neighboring PA₆₃ subunits with a buried surface area of 2,300 Å² (Fig. 5a and c). Although no experiments were conducted on the EF_N–PA interaction for this study, the EF_N structure aligns to

the LF_N of the refined model with an rmsd of 1.7 Å² for 191 Cα atoms, suggesting that EF_N and LF_N bind PA similarly. By contrast, the LF_N-binding site overlaps but is distinct from the PA₂₀-binding sites. PA cannot oligomerize in the presence of PA₂₀ because of steric clash. The model shows that a single LF_N molecule binds across two neighboring PA₆₃ subunits and displaces the PA₂₀ fragments of both subunits. This may explain why ligand binding is so important for PA oligomerization.

The bulk of the LF_N interactions are nonetheless with a single PA₆₃ subunit. There is excellent packing between the PA-binding site on LF_N (Fig. 1a) and the PA ligand-binding subsite I (Fig. 1b) with a significant number of electrostatic interactions (Fig. 5b). The interface also contains a buried His residue contributed by LF_N, H229. The prevalence of charged residues at the interface may be relevant to the pH dependence of the subsequent steps of translocation. The low pH of the endosome triggers conversion of the PA heptameric prepore to the pore and initiates the process of ligand translocation. Low pH also seems to aid the unfolding of LF_N, a process required to transport such a large molecule through the narrow pore lumen (10). Because the enzymatic ligand ultimately needs to be released from the heptamer surface to be translocated, there may be a pH dependence to the binding affinity as well. This pH dependence could be achieved by having a high number of charged and/or titratable residues at the interface.

An electrostatic interaction also may be involved in LF_N's contacts with the PA₆₃–PA₆₃ interface, because the model indicates that LF_N E135 and the K197 residue from the neighboring PA subunit will be in close proximity (Fig. 5a). An attempt to verify this interaction by pairing charge-reversal mutants was unsuccessful (data not shown) but may reflect the fact that PA K197 contributes to the binding interaction from both subunits (Fig. 1b). Despite the lack of direct contacts with R178 and R200 of subsite II, the model does suggest that LF_N spans an interface and structurally occludes the neighboring subunit of PA (Fig. 5c). This occlusion is consistent with the observations that only three molecules of EF/LF/LF_N can bind the heptamer at one time (7) and that the PA₆₃ dimer formed from two nonoligomerizing mutants binds only a single LF_N molecule (16). Finally, the model indicates that the N-terminal α-helix of LF_N is oriented over the luminal space of the PA heptamer (Fig. 5c and d). This helix, corresponding to residues 27–43, represents the first visible part of the LF_N crystal structure, because the N-terminal 26 residues are presumably disordered (12). It has been shown that the N terminus initiates the translocation of LF_N through the lumen of the PA heptameric pore (24). Having LF_N bound such that the N-terminal helix is poised above this opening should facilitate this process and may mean that the N-terminal 26 residues can bind inside the prepore lumen before the beginning of pore formation and translocation (Fig. 5d).

This work was supported by a Charles A. King Trust postdoctoral fellowship (to D.B.L.) and National Institutes of Health Grant AI022021.

- Collier, R. J. & Young, J. A. (2003) *Annu. Rev. Cell Dev. Biol.* **19**, 45–70.
- Leppla, S. H. (1982) *Proc. Natl. Acad. Sci. USA* **79**, 3162–3166.
- Duesbery, N. S., Webb, C. P., Leppla, S. H., Gordon, V. M., Klimpel, K. R., Copeland, T. D., Ahn, N. G., Oskarsson, M. K., Fukasawa, K., Paull, K. D., & Vande Woude, G. F. (1998) *Science* **280**, 734–737.
- Vitale, G., Pellizzari, R., Recchi, C., Napolitani, G., Mock, M., & Montecucco, C. (1998) *Biochem. Biophys. Res. Commun.* **248**, 706–711.
- Molloy, S. S., Bresnahan, P. A., Leppla, S. H., Klimpel, K. R., & Thomas, G. (1992) *J. Biol. Chem.* **267**, 16396–16402.
- Milne, J. C., Furlong, D., Hanna, P. C., Wall, J. S., & Collier, R. J. (1994) *J. Biol. Chem.* **269**, 20607–20612.
- Mogridge, J., Cunningham, K., & Collier, R. J. (2002) *Biochemistry* **41**, 1079–1082.
- Cunningham, K., Lacy, D. B., Mogridge, J., & Collier, R. J. (2002) *Proc. Natl. Acad. Sci. USA* **99**, 7049–7053.
- Gordon, V. M., Leppla, S. H., & Hewlett, E. L. (1988) *Infect. Immun.* **56**, 1066–1069.
- Krantz, B. A., Trivedi, A. D., Cunningham, K., Christensen, K. A., & Collier, R. J. (2004) *J. Mol. Biol.* **344**, 739–756.
- Zhang, S., Udho, E., Wu, Z., Collier, R. J., & Finkelstein, A. (2004) *Biophys. J.* **87**, 3842–3849.
- Pannifer, A. D., Wong, T. Y., Schwarzenbacher, R., Renatus, M., Petosa, C., Bienkowska, J., Lacy, D. B., Collier, R. J., Park, S., Leppla, S. H., et al. (2001) *Nature* **414**, 229–233.
- Shen, Y., Zhukovskaya, N. L., Guo, Q., Florian, J., & Tang, W. J. (2005) *EMBO J.* **24**, 929–941.
- Elliott, J. L., Mogridge, J., & Collier, R. J. (2000) *Biochemistry* **39**, 6706–6713.
- Lacy, D. B., Mourez, M., Fouassier, A., & Collier, R. J. (2002) *J. Biol. Chem.* **277**, 3006–3010.

16. Mogridge, J., Cunningham, K., Lacy, D. B., Mourez, M. & Collier, R. J. (2002) *Proc. Natl. Acad. Sci. USA* **99**, 7045–7048.
17. Gray, J. J., Moughon, S., Wang, C., Schueler-Furman, O., Kuhlman, B., Rohl, C. A. & Baker, D. (2003) *J. Mol. Biol.* **331**, 281–299.
18. Schueler-Furman, O., Wang, C. & Baker, D. (2005) *Proteins* **60**, 187–194.
19. Benson, E. L., Huynh, P. D., Finkelstein, A. & Collier, R. J. (1998) *Biochemistry* **37**, 3941–3948.
20. Wigelsworth, D. J., Krantz, B. A., Christensen, K. A., Lacy, D. B., Juris, S. J. & Collier, R. J. (2004) *J. Biol. Chem.* **279**, 23349–23356.
21. Zhao, J., Milne, J. C. & Collier, R. J. (1995) *J. Biol. Chem.* **270**, 18626–18630.
22. Wesche, J., Elliott, J. L., Falnes, P. O., Olsnes, S. & Collier, R. J. (1998) *Biochemistry* **37**, 15737–15746.
23. Schueler-Furman, O., Wang, C., Bradley, P., Misura, K. & Baker, D., *Science*, in press.
24. Zhang, S., Finkelstein, A. & Collier, R. J. (2004) *Proc. Natl. Acad. Sci. USA* **101**, 16756–16761.
25. Lacy, D. B., Wigelsworth, D. J., Melnyk, R. A., Harrison, S. C. & Collier, R. J. (2004) *Proc. Natl. Acad. Sci. USA* **101**, 13147–13151.